Prepared for submission to JINST

Conceptual design of a hybrid neutron-gamma detector for study of β-delayed neutrons at the RIB facility of RIKEN

BRIKEN collaboration

A. Tarifeño-Saldivia,*[1,2] J. L. Tain,[2] C. Domingo-Pardo,[2] F. Calviño,[1] G. Cortés,[1] V. H. Phong,[3] A. Riego,[1] J. Agramunt,[2] A. Algora,[2,16] N. Brewer,[4,6] R. Caballero-Folch,[7] P. J. Coleman-Smith,[11] T. Davinson,[8] I. Dillmann,[7] A. Estradé,[8,14,15] C. J. Griffin,[8] R. Grzywacz,[5] L. J. Harkness-Brennan,[10] G. G. Kiss,[3,16] M. Kogimtzis,[11] M. Labiche,[11] I. H. Lazarus,[11] G. Lorusso,[19,9] K. Matsui,[3] K. Miernik,[18] F. Montes,[13,14] A. I. Morales,[2] S. Nishimura,[3] R. D. Page,[10] Z. S. Podolyák,[9] V. F. E. Pucknell,[11] B. C. Rasco,[4,6] P. Regan,[9] B. Rubio,[2] K. P. Rykaczewski,[4] Y. Saito,[3,7] H. Sakurai,[3] J. Simpson,[11] E. Sokol,[20] R. Surman,[17] A. Svirkhin,[20] S. L. Thomas,[12] A. Tolosa,[2] and P. Woods[8]

[1] *Universitat Politècnica de Catalunya (UPC), Barcelona, Spain*

[2] *Instituto de Fisica Corpuscular (CSIC-Universitat de Valencia), E-46071 Valencia, Spain*

[3] *RIKEN Nishina Center, 2-1 Hirosawa, Wako-shi, Saitama 351-0198, Japan*

[4] *Physics Division, Oak Ridge National Laboratory, Oak Ridge, Tennessee 37830, USA*

[5] *Department of Physics and Astronomy, University of Tennessee, Knoxville, Tennessee 37966, USA*

[6] *JINPA, Oak Ridge National Laboratory, Oak Ridge, Tennessee 37831, USA*

[7] *TRIUMF, Vancouver, British Columbia V6T 2A3, Canada*

[8] *University of Edinburgh, EH9 3JZ Edinburgh, United Kingdom*

[9] *Department of Physics, University of Surrey, Guildford GU2 7XH, United Kingdom*

[10] *Department of Physics, University of Liverpool, Liverpool L69 7ZE, United Kingdom*

[11] *STFC Daresbury Laboratory, Daresbury, Warrington WA4 4AD, United Kingdom*

[12] *STFC Rutherford Appleton Laboratory, Chilton OX11 0QX, United Kingdom*

[13] *National Superconducting Cyclotron Laboratory, Michigan State University, East Lansing, Michigan 48824, USA*

[14] *Joint Institute for Nuclear Astrophysics, Michigan State University, East Lansing, Michigan 48824, USA*

[15] *Department of Physics, Central Michigan University, Mount Pleasant, MI 48859, USA*

[16] *Institute for Nuclear Research (MTA Atomki), H-4001 Debrecen, POB.51., Hungary*

[17] *Department of Physics, University of Notre Dame, Notre Dame, IN 46556, USA*

[18] *Faculty of Physics, University of Warsaw, PL-02-093 Warsaw, Poland*

[19] *National Physical Laboratory (NPL), Teddington, Middlesex TW11 0LW, United Kingdom*

[20] *Joint Institute for Nuclear Research, Joliot-Curie 6, 141980 Dubna, Moscow Region, Russia*

E-mail: ariel.esteban.tarifeno@upc.edu

*Corresponding author.

Abstract: The conceptual design of the BRIKEN neutron detector at the radioactive ion beam factory (RIBF) of the RIKEN Nishina Center is reported. The BRIKEN setup is a complex system aimed at detecting heavy-ion implants, β particles, γ rays and β-delayed neutrons. The whole setup includes the Advanced Implantation Detection Array (AIDA), two HPGe Clover detectors and up to 166 ^{3}He-filled counters embedded in a high-density polyethylene moderator. The design is quite complex due to the large number and different types of ^{3}He-tubes involved and the additional constraints introduced by the ancillary detectors for charged particles and γ rays. This article reports on a novel methodology developed for the conceptual design and optimisation of the ^{3}He-counter array, aiming for the best possible performance in terms of neutron detection. The algorithm is based on a geometric representation of two selected detector parameters of merit, namely, the average neutron detection efficiency and the efficiency flatness as a function of a reduced number of geometric variables. The response of the neutron detector is obtained from a systematic Monte Carlo simulation implemented in Geant4. The robustness of the algorithm allowed us to design a versatile detection system, which operated in hybrid mode includes the full neutron counter and two clover detectors for high-precision gamma spectroscopy. In addition, the system can be reconfigured into a compact mode by removing the clover detectors and re-arranging the ^{3}He tubes in order to maximize the neutron detection performance. Both operation modes shows a rather flat and high average efficiency. In summary, we have designed a system which shows an average efficiency for hybrid mode (^{3}He tubes + clovers) of 68.6% and 64% for neutron energies up to 1 and 5 MeV, respectively. For compact mode (only ^{3}He tubes), the average efficiency is 75.7% and 71% for neutron energies up to 1 and 5 MeV, respectively. The performance of the BRIKEN detection system has been also quantified by means of Monte Carlo simulations with different neutron energy distributions.

Keywords: Instrumentation for radioactive beams; Neutron detectors; Detector modelling and simulations I

Contents

1 Introduction

Beta-delayed neutron (β_n) emission is a process that can occur when the neutron separation energy in the daughter nucleus (S_n) is smaller than the energy window for the β-decay (Q_β). For neutron-rich nuclei far from stability, β-delayed neutron emission is the dominant decay process. The probability for a nucleus to emit a delayed neutron (P_n) yields information on both, the β-strength distribution and the level structure of the daughter nucleus [1]. Most of the $\sim$ 3000 neutron-rich nuclei still predicted to exist are expected to be β-delayed neutron emitters. In addition to the importance for nuclear structure, P_n values are among the most important input parameters for calculations of the synthesis of neutron-rich heavy elements by the astrophysical rapid neutron-capture process (r-process) [2]. Determining many yet unmeasured P_n values is critical for testing the conditions of the astrophysical environment, and to provide clues about the sites of the r-process. Consequently, the measurement of β-delayed neutron emission probabilities provides unique information about the nuclear structure in exotic nuclei and contributes to the understanding of the formation of the heavy elements in the universe. P_n values are also important for nuclear technology applications. β-delayed neutron emission plays an important role on the transient response of nuclear reactors

and the quantification of decay heat [3]. Therefore, future reactor designs using advanced fuel compositions will benefit from the improvements on current uncertainties of P_n values.

The most common approach to measure P_n values consists in registering the β decays of a specific nucleus in a β detector (N_β) and the delayed neutrons in a neutron detector (N_n). Thus, for single delayed neutron emission one can write [4]

$$P_{1n} = \frac{\bar{\varepsilon}_\beta}{\bar{\varepsilon}_n} \frac{N_n}{N_\beta}. \tag{1.1}$$

In this equation, $\bar{\varepsilon}_\beta$ and $\bar{\varepsilon}_n$ are the beta and neutron detection efficiencies, respectively, averaged over all β and neutron energies.

Whenever the neutron background rate is comparable to or higher than the delayed neutron rate, it is better to use the number of neutrons correlated with β particles ($N_{\beta n}$) instead of N_β. In that case Eq. 1.1 became

$$P_{1n} = \frac{\bar{\varepsilon}_\beta}{\bar{\varepsilon}'_\beta \bar{\varepsilon}_n} \frac{N_{\beta n}}{N_\beta}, \tag{1.2}$$

where $\bar{\varepsilon}'_\beta$ corresponds to the β efficiency averaged over the neutron unbound states and $\bar{\varepsilon}_\beta$ is the β efficiency averaged over all states.

Examination of equations 1.1 and 1.2 shows that the measured P_n values are strongly dependent on the response of the beta and neutron detectors employed. One of the most common methods to detect neutrons is based on the use of ^{3}He-counters embedded in a moderator material such as polyethylene or high-density polyethylene (HDPE) [5]. In this case, the response of the system has to be optimized in such a way that ε_n becomes as insensitive as possible to the primary neutron energy distribution. This condition needs to be fulfilled over a sufficiently broad neutron energy range, comparable to the expected $Q_{\beta n}$ values involved in the β decays under study. In addition, the average neutron detection efficiency needs to be maximized for the measurement of very exotic species, whose production yields are typically very low. These two requirements can be best accomplished if a sufficiently large number of ^{3}He counters becomes available.

To this aim, an international collaboration has been established, which will enable an ambitious programme for β-delayed neutron measurements at RIKEN (BRIKEN) [6]. The current programme is focused on the first measurement of many single neutron emitters in the mass region from A$\sim$50 to A$\sim$150, high-accuracy P_n measurements of several known nuclei and the first measurements of multiple neutron emitters (β_{2n}, β_{3n}, ...).

The radioactive nuclei of interest will be produced at the radioactive isotope beam factory (RIBF) at RIKEN. At RIBF, ^{238}U beams are accelerated by the Superconducting Ring Cyclotron (SRC) up to energies of $345 MeV/u$ and strike the production target at the entrance of the BigRIPS fragment separator [7]. The first stage of BigRIPS consists of two dipole magnets and a wedge-shaped achromatic degrader placed in between. This setup allows one to perform a first selection of the fission residues according to the difference in magnetic rigidity ($B\rho$) before and after the degrader ($B\rho - \Delta E - B\rho$ method). The particle identification is achieved in the second stage of BigRIPS, through the TOF-$B\rho$-ΔE method. This consists in the measurement, event-by-event, of the time of flight (TOF), the magnetic rigidity and the energy loss (ΔE) in order to deduce the atomic number (Z) and the mass-to-charge ratio A/Q of the isotope [8, 9]. Finally, the secondary beam is slowed down by means of a homogeneus aluminum degrader and stopped in a stack of

six double-sided silicon-strip detectors (DSSSD) called AIDA (Advanced Implantation Detector Array) [10, 11]. The latter is axially surrounded by the BRIKEN neutron detector array, which consists of more than 160 ^{3}He tubes of up to six different types, embedded in a large HDPE-block. Two auxiliary HPGe clover detectors can be optionally inserted from both sides in order to measure γ rays following the β decay. BRIKEN is the world largest system of its kind for the detection of β-delayed neutrons. The BRIKEN detector builds upon the experience gained from previous experiments, such as BELEN at JYFL (Finland) [4, 12] and GSI (Germany) [13], 3Hen at ORNL (USA) [14, 15] and NERO at NSCL-MSU (USA) [16].

In order to cope with the large variety of constituents, the compactness and the geometrical complexity of the full detection ensemble, a robust algorithm has been specially developed in order to design and optimize the distribution of ^{3}He counters inside the HDPE matrix. This article describes a new topological method which is based on a geometric representation of two selected parameters of merit, namely, the average neutron efficiency and the efficiency flatness as a function of a reduced number of geometric degrees of freedom.

The present work is organized as follows. The main performance requirements and hardware available for BRIKEN are summarized in Sec. 2. Sec. 3 is devoted to describe the topological algorithm, the simulation code and the figures of merit used within this work, together with the symmetry aspects related to neutron transport in the HDPE moderator. Sec. 4 covers the optimization study for the hybrid setup. The impact of the neutron energy distribution in the detector response is quantified in Sec. 5 by means of MC simulations corresponding to extreme cases. A second iteration of the optimization for design of the compact mode is presented in Sec. 6. The selected configuration for the BRIKEN neutron detector is considered in Sec. 7. Finally, a discussion of the BRIKEN neutron detector compared to other ^{3}He-based setups and the main results and conclusions of this work are presented in Sec. 8 and 9, respectively.

2 Main performance requirements and available materials

In a 4π neutron counter, the overall neutron efficiency (ε) is defined as the product of the geometric efficiency (ε_G) and the neutron detection efficiency, which depends on the neutron moderation, the geometry and the properties of the counter tube array. Thus, for the BRIKEN detector, the maximum achievable overall efficiency is limited by the geometric efficiency of the moderator (see Fig. 1), which is 98.5% for the compact setup and 97% for the hybrid setup, respectively. Furthermore, the maximum average efficiency achieved in a β-delayed neutron counter reported in the literature to date is 61%, corresponding to the TETRA detector, a hybrid setup using 80 ^{3}He counters [17]. Taking this into account, an average neutron efficiency of 60% is defined as the minimum target value for the present design study. This value of neutron efficiency becomes comparable to the β-detection efficiency of state-of the art β-detectors. Consequently, a design with this characteristic mitigates a limitation of the overall detection sensitivity of the full system due to a poor performance of the neutron detector.

For nuclei with large $Q_{\beta n}$ values populating states at high excitation energies in the daughter nucleus, a strong dependence of the detector efficiency on the neutron energy may become important for the measurement of the P_n value (see eqs. 1.1 and 1.2). However, such transitions are readily suppressed by the effect of the Fermi function. Therefore, according to previous experience [4], a

nearly constant efficiency up to neutron energies of ~1 MeV and small variations up to ~5 MeV represent a reliable assumption. This premise will be confronted with extreme hypothesis for neutron energy spectra (see Sec. 5) in order to quantify its possible impact on the performance of the final BRIKEN detection system.

A setup including high-precision gamma spectroscopy compatible with a flat and high neutron efficiency will benefit several of the measurements proposed in the BRIKEN physics program. The decay channels of the multiple neutron emitters accessible at RIBF can be selected by gating on the measured neutron multiplicity and the characteristic γ rays of the daughter nuclei [14].

In summary, the main performance requirements for the BRIKEN neutron detector are:

1. Neutron efficiency higher than 60% up to 1 MeV.

2. Flat response up to 1 MeV and small variations of the efficiency up to 5 MeV.

3. γ-ray detection capabilities compatible with a flat and high neutron efficiency.

To fulfill the requirements of high efficiency and flat response, a large number of ^{3}He -filled neutron counters is mandatory. ^{3}He -filled tubes are very efficient counters for thermal neutrons because of the high cross section of the capture reaction ^{3}He(n,p)^{3}H ($\sigma_{th} = 5345\ barn$, $Q = 764\ keV$) [18]. At epithermal or fast energies, neutron moderation is necessary to achieve high detection efficiencies. The properties of the ^{3}He tubes available in the BRIKEN collaboration are listed in Table 1. Some of these tubes have been used in previous setups for β-delayed neutron detectors such as BELEN [4, 12, 13, 19], 3Hen [14, 15] and TETRA [17, 20].

A HDPE moderator is used for the BRIKEN detector. The moderator has a total size of $90 \times 90 \times 75\ cm^3$ and is composed of 15 HDPE slices of 5 cm thickness. The slices are assembled together by using stainless steel rods passing along the corners of each slice. Depending on the experimental background conditions, the moderator will be shielded using additional HDPE slices, cadmium layers and flexible boron rubber material. In addition to that, the use of veto NaI(Tl) and/or plastic counters is also being considered, and will be tested during commissioning at RIKEN.

γ-ray detection capabilities are implemented at BRIKEN by two large volume HPGe segmented detectors (clovers) embedded into the HDPE moderator. This operation mode is known as the **hybrid mode**. The clover detectors are of the CARDS array type and allow for high-precision gamma spectroscopy [21]. In the hybrid mode, each clover has a total photopeak efficiency of $\sim$ 1% at 1.33 MeV. In general, the performance of HPGe detectors is affected by fast neutrons when the total fluence on the detector is high enough. Resolution degradation has been observed for fluencies higher than $10^9 n/cm^2$ [22]. For the BRIKEN detector, radiation damage on the clovers is not expected due to the very low β-delayed neutron flux produced by the radioactive beams. A very optimistic estimation of the total fluence is $10^6 n/cm^2$ achieved during all the expected campaigns with the BRIKEN detector.

The neutron efficiency may be limited by the clovers embedded into the HDPE moderator. Therefore, the flexibility to transform the hybrid mode into a 4π neutron counter is also a design requirement of the BRIKEN detector. This flexibility is achieved by a mechanical setup allowing the easy removal of the clover detectors in order to fill up the empty space with HDPE plugs and additional ^{3}He tubes. This operation mode is known as **compact mode**.

Table 1. Parameters of the available ^{3}He-filled tubes for the BRIKEN neutron counter.

Detector type	Manufacturer	Pressure (atm)	Tube diameter (inch/cm)	Tube length (inch/cm)	Active length (inch/cm)	Previous setup	Number of counters
B	LND Inc.	8	1.0/2.54	26.61/67.6	23.62/60.0	BELEN	42
R		10	1.0/2.54	26.61/67.6	23.62/60.0	[4, 12, 26]	10
I	GE Reuter Stokes	10	1.0/2.54	29.37/74.6	24.0/60.96	3Hen [15]	17
K		10	2.0/5.08	27.48/69.79	24.0/60.96		64
E		5	1.0/2.54	15.6/39.63	11.18/30.0	—	26
N	—	4	1.18/3.0	23.62/60	19.69/50.0	VASSILISSA [27]	20
Total counters for the BRIKEN detector							**179**

A special data acquisition system (DACQ) has been developed for the BRIKEN setup. A detailed description of this system is provided in Refs. [4, 23, 24]. The DACQ is a self-triggered data acquisition system based on VME digitizers type SIS3302 (8 channels, 100 MSamples/s, 16 bit) and SIS3316 (16 channels, 250 MSamples/s, 14 bit), both from Struck Innovative Systeme [25]. The DACQ is able to handle multiple VME crates and up to 192 channels running independently. By using the on-board processing capabilities of the digitizers, a timestamped readout with the signal amplitude is obtained for each channel. The timestamp is provided by a common time reference distributed to all involved detection systems (BRIKEN counter, AIDA and beam diagnosis detectors).

3 The topological Monte Carlo optimization algorithm

Apart from the large number of detection elements, the precise geometric arrangement of the ^{3}He tubes represents the key feature to achieve both, high and flat neutron detection efficiency over a broad neutron energy range. The optimization of a system combining different tube sizes and diameters, and such a large number of counters is a rather complex and time consuming task. Extensive MC simulations are required and the optimal solution is not necessarily unique. In addition, technical constraints such as construction tolerances, minimum distance between tubes for sufficient mechanical stability and tube alignment make the optimization problem even more complex and challenging.

In order to deal with these difficulties, a methodology based on the optimization of a geometrically parameterized counter array distribution is proposed. In first instance, the parameters of merit are defined (see Sec. 3.2) in order to guide the selection of the most convenient configuration, according to some specific physics requirements. The shape of the array builds upon the symmetries associated to the process of transport and moderation of neutrons in the HDPE (see Sec. 3.3). Secondly, a mathematical analysis is carried out (see Sec. 3.4) in order to obtain an analytical geometric description, which describes any feasible distribution of a certain number of ^{3}He tubes within a given HDPE volume. For this to become effective, the geometry model needs to have as few parameters as possible, typically two or three.

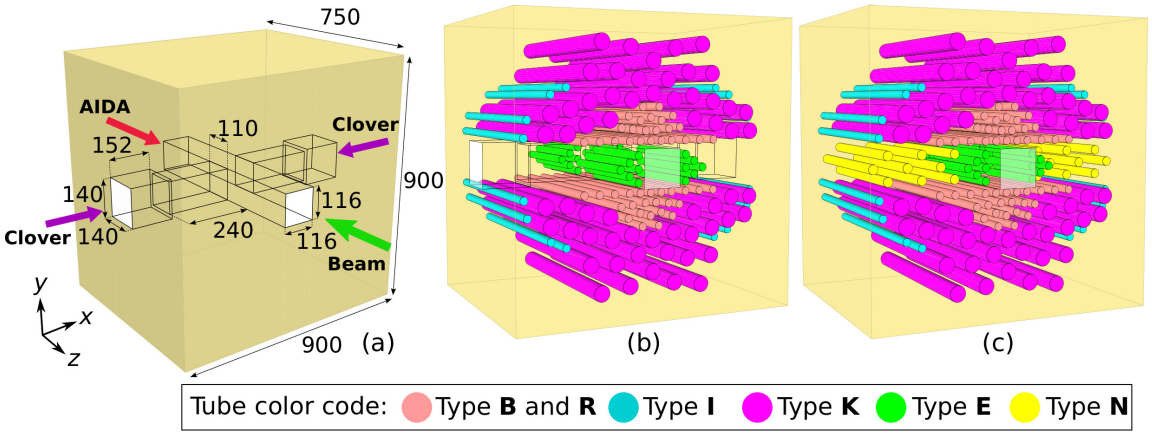

Figure 1. Detector geometries implemented in GEANT4. (a) HDPE moderator geometry for the hybrid mode. Dimensions are in *mm*. Clover detectors are embedded at each side of the moderator along the X axis. The AIDA detector is embedded along the Z axis. (b) and (c) correspond to the counter array distributions for the hybrid (148 tubes) and compact (166 tubes) modes, respectively. For visualization purposes, AIDA and clover detectors are not displayed in the figure, and only active volumes in the ^{3}He counters are shown in (b) and (c).

The MC simulations have been implemented in GEANT4 version 10.0.3 [28]. Data libraries provided by default with this version have been used. The calculations were carried out on a desktop computer running on UBUNTU 14.04 with g++ version 4.8.4. Currently, GEANT4 calculations using neutron proportional counters moderated with HDPE results in good agreement with calculations using the standard code MCNPX (Monte Carlo N-Particle eXtended, developed by Los Alamos National Laboratory) and with experimental measurements [29]. In previous versions, there was a systematic bias in the calculated efficiency due to bugs in the interpolation routines of the thermal libraries [30]. Final corrections for these bugs have been introduced in versions 10.0 and later. Benchmark calculations between GEANT4 (10.0.3) and MCNPX (version 2.5) for a simplified BRIKEN geometry have yielded relative differences in the efficiency of less than 1% [31].

The use of two large volume HPGe clover detectors implies that the hybrid configuration is the most complex case in this study. Therefore, we start the design study with the hybrid configuration (see Sec. 4). Counters of type B to E (see Table 1) have been used for this setup because their diameter and length fit better to the geometrical constrains of the HDPE moderator. The response of the optimized hybrid arrays is studied for different neutron spectra in order to identify the best suited configurations for the compact mode (see Sec. 5). Once a suitable hybrid setup has been found, in a second iteration, the compact configuration design will be tackled (see Sec. 6). In this case, tubes of type N have been added to the optimal configuration for the hybrid mode. A further optimization of type N tubes in the counter array is carried out in order to obtain an optimal configuration for the compact setup.

3.1 GEANT4 detector model and simulations

The generic geometry implemented in GEANT4 is presented in Fig. 1. The HDPE moderator matrix for the hybrid setup is shown in Fig. 1a . The central square holes are designed to host both, the

HPGe clover detectors and AIDA. Fig. 1b and Fig. 1c show generic representations of the counter array distributions for the hybrid and compact geometries, respectively. In the detector model, the HDPE density is 0.95 g/cm^3 and the room temperature is set to 293.6 K. The simulation of ^{3}He counters is implemented using active and passive volumes [29]. The material and dimensions for each tube type are defined according to the information provided by the manufacturer in the data sheet. In the simulation, detected events correspond to energy deposition from 150 keV up to 900 keV inside the ^{3}He active volume, this range corresponds to the typical energy window for the ^{3}He counters. The GEANT4 general particle source (GPS) has been used for the implementation of a particle generator for mono-energetic neutrons. The generator is also able to reproduce the energy distributions taken from data libraries or experimental data. The neutrons are emitted isotropically from a point source placed at the center of the moderator (see Fig. 1). For the optimization of the counter array, calculations have been carried out for a set of discrete neutron energies, namely

$$\mathbb{E}_n = \{0.0001, 0.001, 0.01, 0.1, 1.0, 2.0, 3.0, 4.0, 5.0\}, \text{ in MeV.} \tag{3.1}$$

3.2 Parameters of merit

For a neutron energy in the set $\mathbb{E}_n$, the neutron efficiency is calculated from $\varepsilon(E_i)$ =(Detected events)/(Processed neutrons with initial energy E_i). Two figures of merit are defined as a function of a maximum energy limit (E_{max}):

- Average efficiency: Corresponding to the average for the set of discrete energies used in the calculations,

$$\varepsilon_{av}(E_{max}) = \frac{1}{N_{E_i}} \sum_{E_i \leq E_{max}} \varepsilon(E_i), \tag{3.2}$$

  where $E_i \in \mathbb{E}_n$ (see Eq. 3.1) and N_{E_i} is the number of elements in $\mathbb{E}_n$ satisfying the condition $E_i \leq E_{max}$.

- Flatness factor: A measure of the flat response until a maximum energy limit (E_{max}),

$$F(E_{max}) = \frac{Max(\varepsilon(E_i))}{Min(\varepsilon(E_j))}, \tag{3.3}$$

  where $E_i, E_j \in \mathbb{E}_n$ (see Eq. 3.1) and $E_i, E_j \leq E_{max}$.

Uncertainties in the efficiency are estimated from the statistical errors. Uncertainties associated with the flatness are estimated from error propagation for the quotient.

3.3 Symmetry aspects related to neutron transport

Neutrons in the moderator undergo a reduction of their initial energy by multiple scattering with hydrogen nuclei. The capture reactions inside the ^{3}He counters typically start to be significant for moderated energies below $\sim$ 1 eV. The neutrons can also be captured in the moderator through (n, γ) reactions with hydrogen and carbon nuclei. Capture reactions in the wall of the counters are negligible given the small cross sections of the constituent materials (aluminum and stainless steel). Some neutrons escape from the moderator without any capture reaction. As it can be seen in Fig. 2, the main losses of neutrons take place through the holes and the adjacent region for the

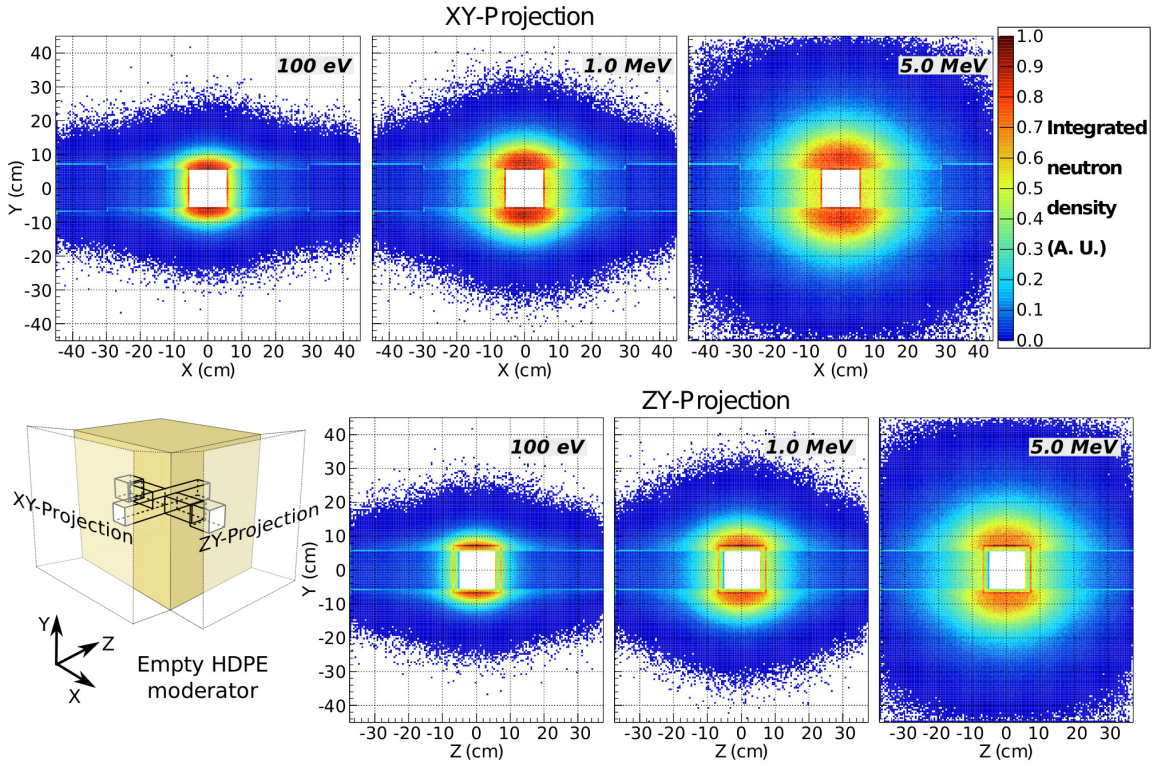

Figure 2. Normalized neutron density inside the HDPE for moderated energies less than 1 eV. Initial neutron energy from left to right: 100 eV, 1.0 MeV, 5.0 MeV. The neutron density integrated over the Z and X axis (XY and ZY-projection) is shown on top and bottom, respectively.

HPGe clover detectors and AIDA, respectively. Thus, the internal geometry of the moderator and the position of the counters in these regions become relevant for the optimization of the BRIKEN detector performance.

In previous compact setups such as NERO, BELEN or 3Hen, the moderator has a central hole to accommodate an implantation system and a β detector. For such a geometry, the counters have been arranged in concentric rings around the central hole. This design concept is motivated by the cylindrical symmetry around the axis hole arising from the moderation of neutrons.

In the BRIKEN moderator, the symmetry around the central hole is modified by the holes for the clover detectors. In order to provide insights on how to arrange the ^{3}He counters, a study of the transport and slowing down of neutrons in the BRIKEN moderator has been carried out using the tracking capabilities of GEANT4. For the study, 4×10^6 neutrons were processed for each initial energies of 100 eV, 1.0 MeV and 5.0 MeV. The neutrons were tracked until they escaped or were captured in the moderator. The last position of the neutron history in the moderator was used to compute a neutron density, moderated energies less than 1 eV are considered for this computation. The results of the study are presented in Fig. 2. The neutron density has been integrated along the Z and X axis (XY and ZY-projection, respectively), and normalized to its maximum value for a qualitative analysis. The effect on the symmetries of the moderation process of the clover holes and the AIDA hole can be observed in Fig. 2 on the XY-projection and the ZY-projection, respectively.

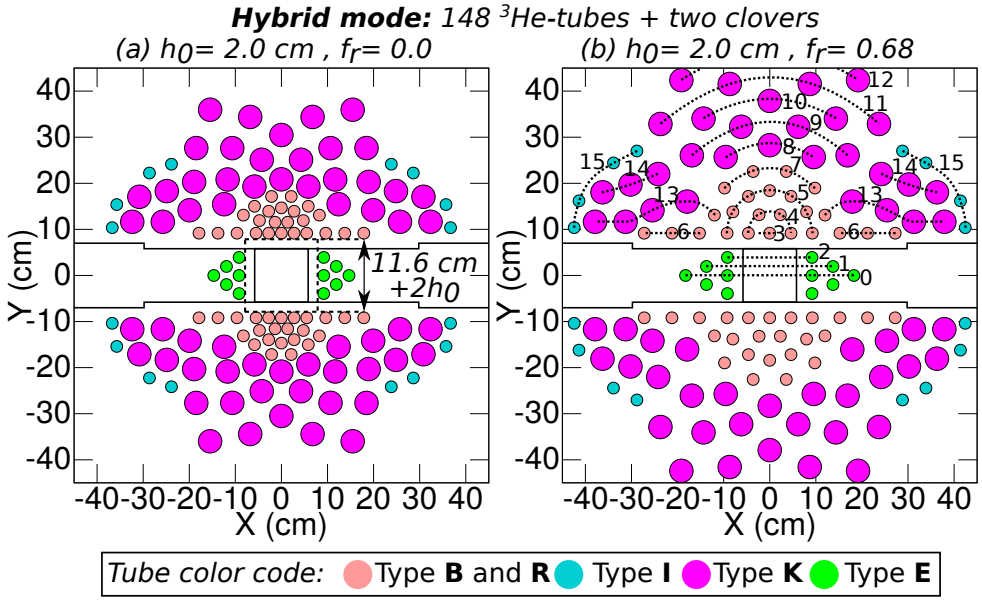

Figure 3. Parameterized counter array distribution for the hybrid mode using 148 ^{3}He-tubes. The size of the central hole is 11.6 cm. The counter array distribution is determined by a set of parametric functions ($\vec{R}_i$) which depend on parameters h_0 and f_r. The parameterization is shown for parameters (a) h_0=2 cm, f_r=0.0; and (b) h_0=2 cm, f_r=0.68. The parametric functions are depicted in (b) for the shell index i : 0 . . . 15 using dotted lines.

In Fig. 2 there are two regions where the neutron density is symmetric: the regions on top and bottom of the holes along the Y axis, and the zone adjacent to the holes in middle of the moderator. In the top and bottom regions, the neutron density has an oval shape. At 100 eV, the neutron density is peaked up to $\sim$ 4 cm from the border of the holes. In contrast at 5 MeV, the peak of the density is broadened up to $\sim$ 15 cm from the border. Beyond this region, the density decreases roughly to a constant value in the external part of the moderator. Consequently, while the counters placed close to the holes are critical to obtain a high efficiency, the counters distributed on the external parts of the moderator are important for a flat response up to 5 MeV. It is worth mentioning that for the first group of counters placed in the internal region of the moderator, the separation distance from the hole borders for AIDA and clovers will also play an important role. This is a consequence of the high neutron density values in this region (see Fig. 2).

3.4 Parameterization of the counter array distribution

Around 5 to 10% of the BRIKEN tubes by type have been reserved as spares, to allow a fast exchange of defective tubes during the experimental campaign. A total of 148 ^{3}He-tubes of type B to E have been used in the counter array distribution for the hybrid mode. Including tubes type N, a total of 166 tubes out of the 179 available (see Table 1) have been used for the counter array in compact mode.

The counter array distributions for the hybrid and compact modes are shown in figures 1b and 1c respectively. For the purpose of visualization, only the active volumes are visible in these

GEANT4 representations of the detector geometry. By symmetry arguments (see section 3.3), the following has been assumed for the parameterization of the counter array distribution:

i. All counters are placed along the Z axis, i.e. in parallel with the AIDA hole axis.

ii. The counter distribution has an oval shape.

iii. The counter distribution is closely-packed around the AIDA hole. Consequently, 1 inch counters are placed in the inner region of the moderator and 2 inch counters are used in the external region. In addition, it is worth mentioning that placing larger-diameter tubes in the peripheral region is a way to minimize the impact a sudden failure of these tubes on the overall detector performance.

For the hybrid mode, as shown in Fig. 1b, tube types B to K (see Table 1) are placed on the top and bottom regions of the moderator. The shorter type E tubes are placed in the zone adjacent to the holes in the middle of the moderator. These tubes are placed backwars and forwards of the clover holes.

For the compact mode, the clover holes are filled up with HDPE. Collinear type E tubes are put in contact at the central plane of the moderator. In addition, tubes of type N are placed next to type E tubes in the central region, as shown in Fig. 1c. Tubes on top and bottom of the moderator remain in the same position as for the hybrid mode.

To facilitate the assembly of the detector in hybrid mode, the tubes are aligned along the Z axis 5 cm from the moderator border. One of the 5 cm HDPE slices is used as the alignment reference for this purpose. The only exception is for type E tubes, for which case the edge of the clover hole is used as the alignment point.

Due to mechanical reasons, a tolerance of 2 mm has been assumed for the cavities housing the tubes in the moderator. In addition, a minimum distance of 5 mm between each cavity has been assumed to constrain the optimization of the counter array distribution.

The parametrization for the hybrid mode using 148 ^{3}He tubes is presented in Fig. 3. This counter array distribution has been achieved by grouping the tubes in "shells" around the hole for AIDA. Such shells are depicted using dotted lines in Fig. 3b for label index $i : 0, \ldots, 15$. Therefore, the position of the j^{th}-counter in the i^{th}-shell is determined in the XY-plane by parametric functions with the form,

For $i : 0, 1, 2$ and $j : 1, \ldots, n_i$, in cartesian coordinates:

$$\vec{R}_{i,j} = \hat{y} \cdot (P_{0,i} + P_{1,i} \cdot f_r + P_{2,i} \cdot i) + \hat{x} \cdot (h_0 + p_{0,i} + p_{1,i} \cdot f_r + \Delta_{i,j} \cdot j) \tag{3.4}$$

For $i : 3, \ldots, 15$ and $j : 1, \ldots, n_i$, in polar coordinates:

$$\vec{R}_{i,j} = \hat{r} \cdot (h_0 + P_{0,i} + (i-3) \cdot (P_{1,i} \cdot f_r + P_{2,i})) + \hat{\theta} \cdot (p_{0,i} + \Delta_{i,j} \cdot j) \tag{3.5}$$

Where $P_{0,i}$, $P_{1,i}$, $P_{2,i}$, $p_{0,i}$, $p_{1,i}$, and $\Delta_{i,j}$ are constants for the parameterization, n_i is the number of tubes in the i^{th}-shell, h_0 is the separation in cm from the inner moderator border to the first shell next to the hole (see Fig. 3a), and f_r is a dimensionless spacing parameter.

In general, for a given shell, the spacing between tubes depends on n_i and f_r. In addition, the space between shells depends also on f_r. Provided the setting of n_i for each shell ($\sum_i n_i = 148$

for the hybrid mode), the impact of f_r on the tube spacing and shell separation for the proposed parameterization is presented in figures 3a and 3b.

4 Hybrid BRIKEN design

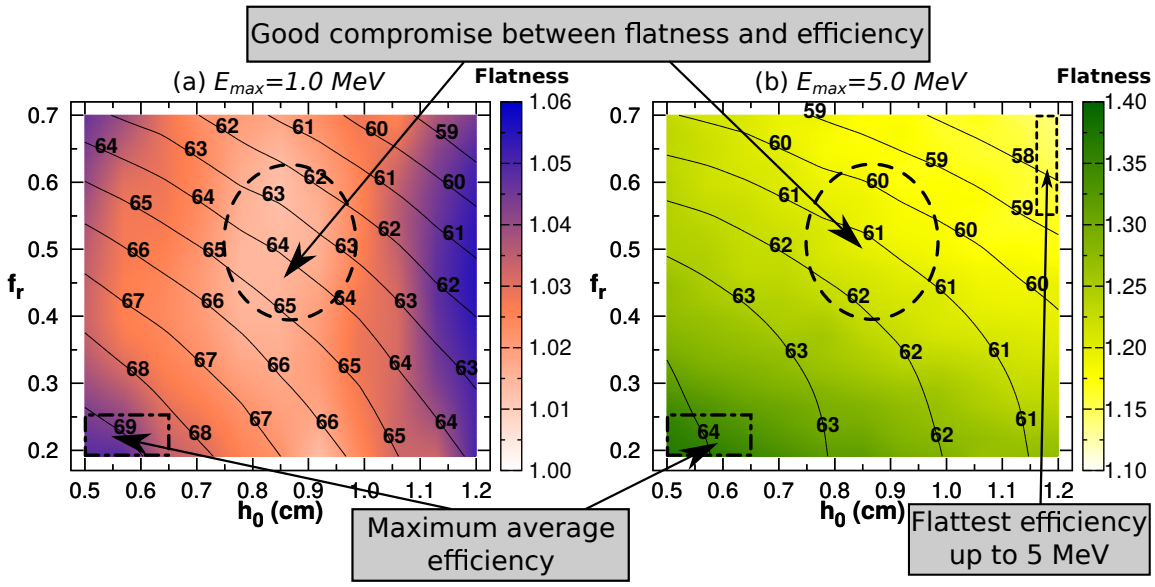

Figure 4. Average efficiency (Eq. 3.2) and flatness (Eq. 3.3) in the parameter space (h_0, f_r) for the hybrid mode. The average efficiency is displayed in percentage points with lines and the flatness as a colour map. In (a) results for $\varepsilon_{av}(1\ MeV)$ and $F(1\ MeV)$ are shown, while in (b) results for $\varepsilon_{av}(5\ MeV)$ and $F(5\ MeV)$ are presented. The region for maximum average eficiency is found on the bottom left part in (a) and (b), the good compromise region between flatness and efficiency is found on the central region in (a) and (b), and the flattest efficiency region up to 5 MeV is the small area on the top right in (b).

Calculations of efficiency and flatness for the parametric counter array presented in Sec. 3.4 have been carried out. The calculations were done for the parameter space (h_0, f_r). Constraining the computations by the minimum separation between the tube housing cavities results in parameter ranges for calculation of $0.19 \leq f_r \leq 0.70$ and $0.5\ cm \leq h_0 \leq 1.2\ cm$. The parameter space was divided into a grid of 11×21 points. A total of 50000 neutron histories were processed for each point in the grid and the set of discrete neutron energies in Eq. 3.1. Such statistics allow one to identify regions of interest in the parameter space, while keeping the total computational time within a reasonable limit.

The results of the calculations are presented in Fig. 4. In these calculations, the typical statistical uncertainty for the flatness values are $\Delta F(1\ MeV) \approx \pm 0.008$ and $\Delta F(5\ MeV) \approx \pm 0.01$. For neutrons up to 1 MeV, a very flat response ($F(1\ MeV) < 1.1$) is obtained with the average efficiency ranging from 58% up to 69%. For neutrons up to 5 MeV, a compromise between the average efficiency and flatness is observed, the greater the flatness the lower the efficiency. The average efficiency ranges from 56% to 64%, while the flatness value is $1.13 < F(5\ MeV) < 1.4$. Comparing calculations results up to 1 and 5 MeV, three regions of interest for optimization

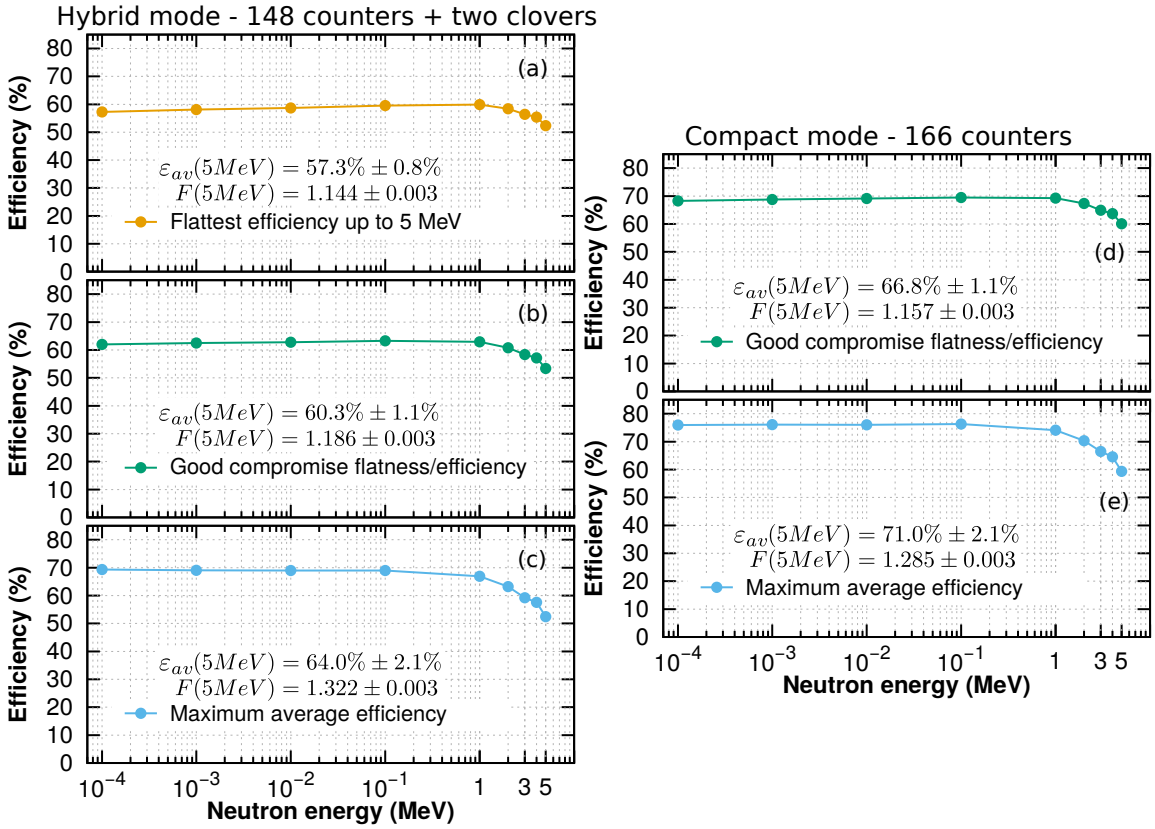

Figure 5. Neutron responses for optimized configurations. (a), (b) and (c) are for the hybrid mode using 148 counters and two clovers. (d) and (e) are for the compact mode using 166 counters without clovers.

have been identified; (i) the region of flattest efficiency up to 5 MeV, (ii) the region with a good compromise between efficiency and flatness up to 1 and 5 MeV, and (iii) the region of maximum efficiency up to 1 and 5 MeV. These regions are depicted with dashed lines in Fig. 4.

Calculations with increased statistics (500000 neutron histories) were carried out for the configurations in the above mentioned regions of interest. By doing so the flatness uncertainty decreased to a level, which was low enough for the optimization purpose ($\Delta F(5\ MeV) \lesssim \pm 0.003$). Finally, the optimized configuration for each region was obtained by maximizing the average efficiency and minimizing the flatness value in the calculations up to 5 MeV. The neutron responses for the three optimized configurations are shown in figures 5a-c. The parameters of the optimized configurations are reported in Table 2.

5 Impact of the neutron energy spectrum

The response of the optimized configurations to different neutron spectra has been studied to identify which configuration is better suited for optimization of the compact mode. With this in mind, the efficiency has been calculated for two representative decays with a *soft* and *hard* neutron spectrum for medium-heavy nuclei. The *soft* spectrum is shown in Fig. 6a and corresponds to the ENDF/B-VII.1 spectrum of β-delayed neutrons in ^{88}Br [18]. The *hard* spectrum is shown in Fig. 6b and

Table 2. Parameters of the optimized hybrid configurations (148 ^{3}He tubes + 2 clovers) and response to different neutron spectra. In columns 2 and 3, h_0 and f_r are the counter array distribution parameters (Sec. 3.4). In column 4, *F(5 MeV)* is the flatness calculated up to 5 MeV (Eq. 3.3). In columns 5 and 6, $\frac{\varepsilon(^{84}Ga)}{\varepsilon(^{88}Br)}$ and $\frac{\varepsilon(^{252}Cf)}{\varepsilon(^{88}Br)}$ are the efficiency ratios for neutron spectra ^{84}Ga and ^{252}Cf over ^{88}Br, respectively. Finally in columns 7 and 8, ε_{1n} and ε_{2n} correspond to the estimated efficiency for one and two *beta*-delayed neutrons, respectively.

Configuration	h_0 (cm)	f_r	$F(5\ MeV)$	$\frac{\varepsilon(^{84}Ga)}{\varepsilon(^{88}Br)}$	$\frac{\varepsilon(^{252}Cf)}{\varepsilon(^{88}Br)}$	ε_{1n}	ε_{2n}
Flattest efficiency up to $5MeV$	1.2	0.649091	1.144	1.000 ± 0.003	0.963 ± 0.003	59.8%	35.8%
Good compromise flatness/efficiency	0.92	0.547273	1.186	1.002 ± 0.003	0.947 ± 0.002	63.3%	40.1%
Maximum efficiency up to 1 *and* $5MeV$	0.57	0.267273	1.322	0.996 ± 0.003	0.908 ± 0.002	68.6%	47.0%

resembles the one measured for the decay of ^{84}Ga with the VANDLE neutron detector [32, 33]. It is important to emphasize that both spectra have a similar average energy ($\bar{E}_n \approx 250 - 300\ keV$), although a significant portion of the *hard* spectrum extends beyond 1.5 MeV in the ^{84}Ga decay.

The efficiency for a ^{252}Cf neutron source (Fig. 6c) has been also calculated. The neutron energy distribution has been sampled from the prompt fission Watts spectrum [34]. This spectrum is too hard for a β-delayed neutron emitter (sample mean $\bar{E}_n = 2.28\ MeV$), but it is commonly used for calibration of neutron detectors based on moderated proportional counters. Thus, the calculation of the ^{252}Cf efficiency provides a conservative estimate of the maximal deviation due to the hardness of the spectrum. In addition, it provides a reference of the expected efficiency for an experimental characterization of the detector.

The results of the calculations are reported in Table 2. For each optimized configuration, the ratio of efficiencies $\varepsilon(^{84}Ga)/\varepsilon(^{88}Br)$ (*hard* to *soft* spectrum) and $\varepsilon(^{252}Cf)/\varepsilon(^{88}Br)$ are presented. In addition, estimates of the efficiency for single (ε_{1n}) and double (ε_{2n}) β-delayed neutron emission are also presented. For single emission, ε_{1n} corresponds to the efficiency averaged for ^{88}Br and ^{84}Ga. For double emission, the efficiency is estimated from $\varepsilon_{2n} = \varepsilon_{1n}^2$. Inspection of Table 2 shows that the methodology presented in this work has led to optimized configurations with a very flat response for both representative β-delayed neutron spectra. Even for the harder spectra from a ^{252}Cf source, deviations less than 10% are obtained for all the optimized configurations. When comparing results for the ratio $\varepsilon(^{84}Ga)/\varepsilon(^{88}Br)$, ε_{1n} and ε_{2n} in Table 2, a poorer performance is observed for the flattest efficiency configuration with respect to the others. Therefore, the flattest efficiency configuration is excluded from the further analysis for optimization of the detector in compact mode.

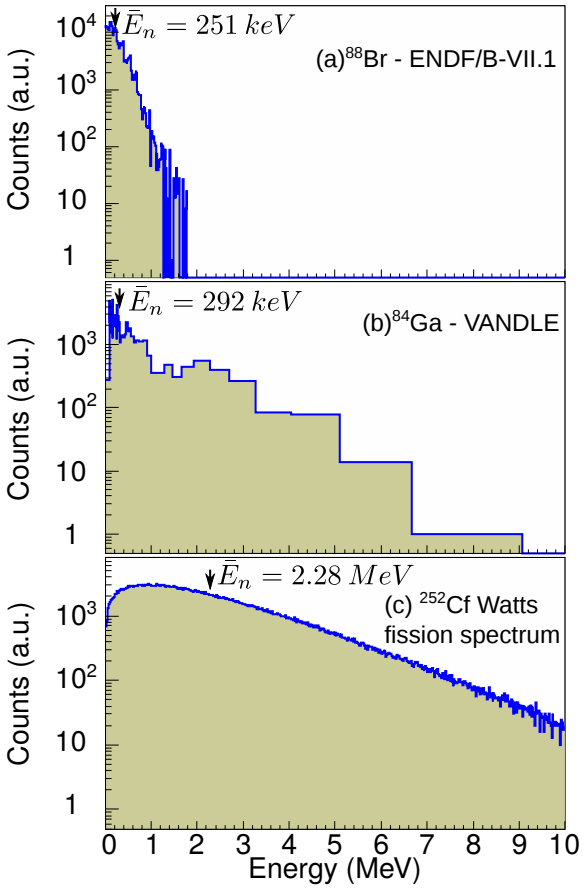

Figure 6. Different neutron-energy spectra simulated. (a) β-delayed neutron spectrum of ^{88}Br from ENDF/B-VII.1 [18]. (b) resembles the ^{84}Ga β-delayed neutron spectrum measured using the VANDLE detector [32, 33]. (a) and (b) are representative of *soft* and *hard* β-delayed neutron spectra. (c) is the neutron-energy spectrum for a ^{252}Cf source derived from the Watts fission spectrum [34].

Table 3. Parameters of the optimized compact configurations (166 ^{3}He tubes) and response to different neutron spectra. In column 2 g_r corresponds to the array distribution parameter for compact mode (Sec. 6).

Configuration	g_r	*F(5MeV)*	$\frac{\varepsilon(^{84}Ga)}{\varepsilon(^{88}Br)}$	$\frac{\varepsilon(^{252}Cf)}{\varepsilon(^{88}Br)}$	ε_{1n}	ε_{2n}
Good compromise flatness/efficiency	0.57	1.157	1.004 ± 0.002	0.957 ± 0.002	69.6%	48.4%
Maximum efficiency up to 1 *and* 5*MeV*	0.75	1.285	0.999 ± 0.002	0.916 ± 0.002	75.8%	57.5%

6 Compact BRIKEN design

The transformation from hybrid to compact mode is achieved by removing both clover detectors and filling up the empty space with HDPE plugs. The Z position of concentric type E tubes are modified by putting both ends in contact. As shown in Fig. 1c, additional tubes of type N are placed in the central region of the moderator. A further optimization of the configuration of these tubes has been carried out. For this purpose, the XY-positions of type N tubes have been parameterized separately for the configurations *good compromise flatness/efficiency* and *maximum efficiency*. These parameterizations introduce a new parameter (g_r) which defines the horizontal separation between the tubes in the XY-plane. Along the Z axis, the active volumes of type N tubes are centered with respect to the center of the moderator. Eighteen tubes have been used for the new parameterization. Thus, a total of 166 ^{3}He tubes are used for the compact mode.

The parameter calculation range for the optimization of the compact mode was $0.21 \leq g_r \leq 0.81$. The optimization procedure is similar to that used for the hybrid mode. Two optimized configurations have been obtained for the compact mode. The optimized parameters are presented in Table 3. The neutron energy response for each optimized configuration is presented in figs. 5d and 5e. Examination of these results reveals that the transformation from the hybrid to compact mode yields an improvement in the flatness of the neutron response and the magnitude of the efficiency. In fact, for both configurations, the flatness value has a relative decrease of around 3% and the neutron efficiency has an absolute increase of around 6%.

The responses of both optimized configurations to different neutron spectra have been also studied. Results of these calculations are presented in Table 3. The improvements of the flatness and efficiency for compact mode are also reflected when comparing Tabs. 2 and 3. In fact, there is an increase of the ratio $\varepsilon(^{252}Cf)/\varepsilon(^{88}Br)$ towards unity for the compact mode. In contrast, the ratio $\varepsilon(^{84}Ga)/\varepsilon(^{88}Br)$ remains constant for both modes.

7 Selected configuration for the BRIKEN neutron detector

Two possible optimized configurations have been proposed for the BRIKEN neutron detection system in hybrid mode. Both configurations can be transformed into the compact mode, which yields an overall increase of the efficiency and a slightly flatter neutron response. The performance of these two configurations, namely *good compromise flatness/efficiency* and *maximum efficiency*, is summarized in Fig. 5 and Tabs. 2 and 3. The *Good compromise flatness/efficiency* configuration has a flatter response than *maximum efficiency* configuration. However, a negligible impact is found when comparing the performances for the two representative β-delayed neutron spectra (^{88}Br and ^{84}Ga) in either hybrid and compact modes. For the harder ^{252}Cf fission spectrum, the efficiency decreases less than 10% in relative terms for both configurations. When comparing the estimated values for ε_{1n} and ε_{2n}, a clear advantage of the *maximum efficiency* configuration for the compact mode is shown, which offers the possibility obtaining an efficiency close to 58% for double neutron emission.

The BRIKEN collaboration has chosen the *maximum efficiency* configuration as the final setup for the BRIKEN neutron detector. This decision has been made based upon the physics program, the arguments outlined above and the technical advantages of each configuration. To summarize,

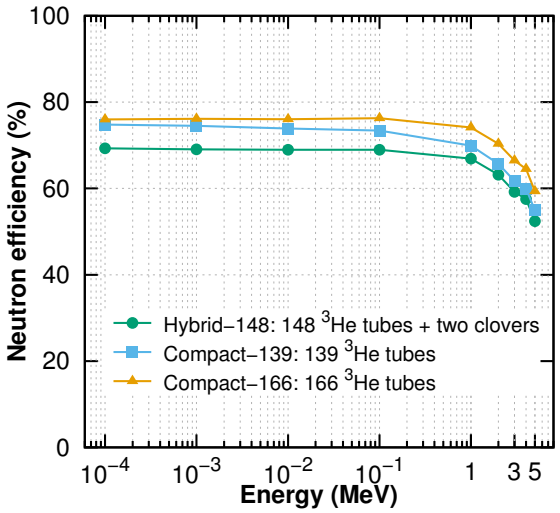

Figure 7. Neutron response of the final configuration for operational modes hybrid (148 tubes + two clovers) and compact (166 tubes). An additional compact configuration using 148 tubes is also shown for comparison.

the neutron response of the final configuration for both operational modes are presented in Fig. 7. An optional configuration for compact mode using only the 148 counters is also presented. This configuration is the compact one just obtained without using type N tubes. As can be seen from Fig. 7, by transforming the setup into the compact mode with 148 tubes, the efficiency is increased in around 4.5% absolute from lower energies up to 1 MeV, but the flatness is impaired. The addition and optimization of type N tubes increases the efficiency up to 5 MeV and helps to recover the flat response.

8 Discussion

A review of the neutron performance of the BRIKEN detector in its final configuration and other setups for β-delayed neutrons is presented in Table 4. In addition, the average efficiencies for setups separated into hybrid and compact modes are plotted in Fig. 8. For each detector, neutron response functions from MC calculations have been reported in refs. [4, 15–17, 35]. These functions are used for calculation of data presented in Table 4. It is worth mentioning that this table summarizes most of the setups using ^{3}He counters for β-delayed neutron measurements reported during the last fifteen years.

Each detector in Table 4 has been designed addressing different technical requirement for the geometric setup, efficiency and flatness. Nevertheless, as shown in Fig. 8, the roughly trend for hybrid and compact setups is the greater the number of tubes, the greater the neutron efficiency. The only exception to this trend is BELEN-20 detector, where the setup was optimized to enhance the neutron detection efficiency [4]. Additionally, comparison of the BRIKEN compact-148 and compact-166 configurations indicate that no important increase of the neutron efficiency can be achieved by adding more counters to the configuration.

Table 4. Comparison of different β-delayed neutron setups reported during the last fifteen years. In columns 4 and 6, the flatness calculated up to neutron energies of 1 and 5 MeV, respectively. In columns 5 and 7, the efficiency averaged up to neutron energies of 1 and 5 MeV, respectively.

Detector	Number of counters	Setup type	$F(1\ MeV)$	$\varepsilon_{av}(1\ MeV)$	$F(5\ MeV)$	$\varepsilon_{av}(5\ MeV)$
	166	Compact	1.029	75.7%	1.285	71%
BRIKEN	148	Compact	1.07	73.3%	1.362	67.6%
	148	Hybrid	1.036	68.6%	1.322	64.0%
TETRA [17]	80	Hybrid	1.133	61.1%	1.842	51.6%
MAINZ** [35]	64	Compact	1.130	47.0%	2.245	39.9%
NERO [16]	60	Compact	1.157	43.1%	1.926	38.3%
Hybrid-3Hen [15]	48	Hybrid	1.103	36.8%	1.781	32.5%
BELEN-20 [4]	20	Compact	1.062	46.2%	1.620	41.1%
LOENI** [35]	18	Hybrid	1.016	17.4%	1.645	16.1%

**Neutron response extrapolated for energies higher than 2 MeV.

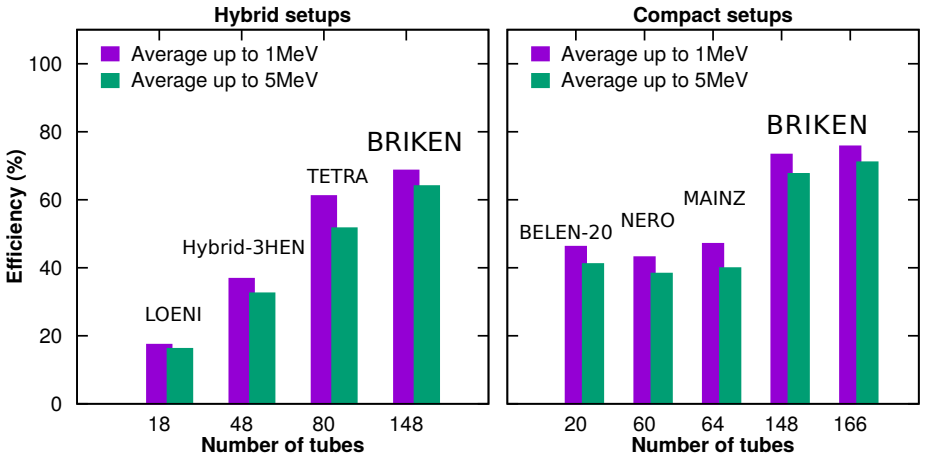

Figure 8. Efficiencies of hybrid and compact β-delayed neutron setups reported during the last fifteen years. For visualization purposes, the axis for number of tubes is not to scale.

According to the publications, most β-delayed neutron detectors have been designed to have a nearly flat response up to 1 MeV. This is also reflected by the values of $F(1\ MeV)$ in Table 4. The flattest response for this energy range in the table corresponds to LOENI detector, which was specially designed to have an energy-independent efficiency [35]. In second place appears the BRIKEN detector with a $F(1\ MeV)$ value similar to LOENI, but an average efficiency up to 1 MeV four times higher. This fact highlights the impact of using a large number of neutron detectors and the optimization methodology presented in this work.

One of the most interesting features of the BRIKEN neutron detector arises from examination of the flatness up to 5 MeV. The BRIKEN compact-166 and hybrid-148 configurations exhibit the

flattest response in this energy range in comparison with other detectors in Table 4. The relative difference in $F(5\ MeV)$ values is significant, starting from around 25% for LOENI and BELEN-20, up to 72% in the case of the Mainz long counter. Moreover, the average efficiency up to 5 MeV of the BRIKEN detector is still the highest. Thus, the BRIKEN neutron detector is found to be the best compromise between high efficiency and flat response on Table 4. To summarize, the high neutron efficiency, flat response up to 5 MeV, γ-ray detection capabilities and the flexibility of the setup make the BRIKEN neutron detector the state-of-the-art in detectors for β-delayed neutrons.

9 Summary and final remarks

The conceptual design of the BRIKEN neutron counter is reported. This new system has been designed to measure β-delayed neutron emission properties of a large number of very neutron-rich nuclei produced at the RIKEN Nishina Center in Japan. In order to facilitate the design of the detector, a topological Monte Carlo optimization algorithm has been developed and implemented in GEANT4. This methodology is based on the study of the transport and slowing down of neutrons in the HDPE moderator, the use of this information for parameterization of the counter array distribution, and the optimization of the array for high efficiency and flat response.

The design concept of the BRIKEN neutron detector is flexible and allows the detector to be operated in hybrid and compact modes, whilst keeping a high efficiency and a nearly constant neutron response. In hybrid mode, the setup is composed of 148 ^{3}He tubes and two clover detectors for high-precision γ spectroscopy ($\sim$ 1% total photopeak efficiency at 1.33 MeV for each clover). In compact mode, the setup is composed of 166 ^{3}He tubes and operates as a 4π neutron counter. The transformation from one mode to the other can be achieved easily between experimental runs.

The response functions for both operational modes are very flat up to 1 MeV and decrease slowly at higher energies. For example at 5 MeV, the relative decrease of the efficiency is less than 25%. Moreover, for two representative spectra such as the β-delayed neutron emitter ^{88}Br ($\bar{E}_n = 251\ keV$) and the harder neutron spectrum from fission of ^{252}Cf ($\bar{E}_n = 2.28\ MeV$), a relative decrease in the efficiency of less than 10% is found. For such a flat neutron response, the estimated efficiencies for single β-delayed neutrons in hybrid and compact mode are around 68.6% and 75.8%, respectively. Thus, efficiencies as high as 57.5% can be obtained for double neutron emission. The high efficiency of the detector is essential to allow measurements on very neutron-rich isotopes with very low production rates.

The BRIKEN neutron detector is the result of a joint effort to build a state-of-the-art detector for the most exotic β-delayed neutron emitters. This setup is going to be used for precise β-delayed neutron measurements in very short-lived nuclei. For this purpose, a collaboration involving 20 institutions from different countries has been established. The HDPE moderator has been built during the first quarter of 2016 based on the design reported in this work. The full assembly and characterization of the BRIKEN detector has been completed by the end of 2016.

Acknowledgments

This work has been supported by Spanish Ministerio de Economia y Competitividad under grants FPA2008-04972-C03-03, FPA2011-28770-C03-03, FPA2011-24553, FPA2014-52823-C2-

1-P, FPA2014-52823-C2-2-P and the program Severo Ochoa (SEV-2014-0398). Work supported by the European Commission under the FP7/EURATOM CHANDA contract 605203. Work partially done within the IAEA-CRP for Beta Delayed Neutron Data. G. G. Kiss acknowledges support from OTKA (K120666) and JSPS (KAKENHI 2604808).

References

[1] I. N. Borzov. Beta-delayed neutron emission in the ^{78}Ni region. *Phys. Rev. C*, 71:065801, Jun 2005. doi: 10.1103/PhysRevC.71.065801.

[2] A. Arcones and G. Martínez-Pinedo. Dynamical r-process studies within the neutrino-driven wind scenario and its sensitivity to the nuclear physics input. *Phys. Rev. C*, 83:045809, Apr 2011. doi: 10.1103/PhysRevC.83.045809.

[3] I. Dillmann, B. Singh, and P. Dimitriou. Development of a Reference Database for Beta-Delayed Neutron Emission. Summary Report NDC(NDS)-0683 (2015).

[4] J. Agramunt, J. L. Tain, M. B. Gómez-Hornillos, A. R. Garcia, F. Albiol, A. Algora, R. Caballero-Folch, F. Calviño, D. Cano-Ott, G. Cortés, C. Domingo-Pardo, T. Eronen, W. Gelletly, D. Gorelov, V. Gorlychev, H. Hakala, A. Jokinen, M. D. Jordan, A. Kankainen, V. Kolhinen, L. Kucuk, T. Martinez, P. J. R. Mason, I. Moore, H. Penttilä, Zs. Podolyák, C. Pretel, M. Reponen, A. Riego, J. Rissanen, B. Rubio, A. Saastamoinen, A. Tarifeño-Saldivia, and E. Valencia. Characterization of a neutron-beta counting system with beta-delayed neutron emitters. *Nucl. Instrum. And Meth. in Phys. Res. A*, 807:69–78, 2015.

[5] P. L. Reeder, J. F. Wright, and L. J. Alquist. Average neutron energies from separated delayed-neutron precursors. *Physical Review C*, 15(6):2098, 1977.

[6] BRIKEN collaboration. https://www.wiki.ed.ac.uk/display/BRIKEN/Home.

[7] T. Kubo. In-flight RI beam separator BigRIPS at RIKEN and elsewhere in Japan. *Nuclear Inst. And Methods in Physics Research, B*, 204:97 – 113, 2003. doi: http://dx.doi.org/10.1016/S0168-583X(02)01896-7.

[8] T. Kubo, D. Kameda, H. Suzuki, N. Fukuda, H. Takeda, Y. Yanagisawa, M. Ohtake, K. Kusaka, K. Yoshida, N. Inabe, T. Ohnishi, A. Yoshida, K. Tanaka, and Y. Mizoi. BigRIPS separator and ZeroDegree spectrometer at RIKEN RI Beam Factory. *Prog. Theor. Exp. Phys.*, 2012(1):03C003, 2012. doi: 10.1093/ptep/pts064.

[9] N. Fukuda, T. Kubo, T. Ohnishi, N. Inabe, H. Takeda, D. Kameda, and H. Suzuki. Identification and separation of radioactive isotope beams by the BigRIPS separator at the RI beam factory. *Nuclear Inst. And Methods in Physics Research, B*, 317:323 – 332, 2013. doi: http://dx.doi.org/10.1016/j.nimb.2013.08.048.

[10] AIDA collaboration. Technical Report For the Design, Construction and Commissioning of the Advanced Implantation Detector Array (AIDA). http://www2.ph.ed.ac.uk/~td/AIDA/Design/tdr_aida.pdf.

[11] C. Griffin, T. Davinson, A. Estrade, D. Braga, I. Burrows, P. Coleman-Smith, T. Grahn, A. Grant, L. J. Harkness-Brennan, M. Kogimtzis, I. Lazarus, S. Letts, Z. Liu, G. Lorusso, K. Matsui, S. Nishimura, R. D. page, M. Prydderch, V. F. E. Pucknell, S. Rinta-Antila, O. J. Roberts, D. A. Seddon, J. Simpson, J. Strachan, S. L. Thomas, and P. J. Woods. Beta-Decay Studies of R-Process Nuclei Using the Advanced Implantation Detector Array. In *Proceedings of XIII Nuclei in the Cosmos (NIC XIII), PoS(NIC XIII)097*, 2014.

[12] J. Agramunt, A.R. Garcia, A. Algora, J. Äystö, R. Caballero-Folch, F. Calvino, D. Cano-Ott, G. Cortes, C. Domingo-Pardo, T. Eronen, and Others. New beta-delayed neutron measurements in the light-mass fission group. *Nuclear Data Sheets*, 120:74–77, 2014.

[13] R. Caballero-Folch, C. Domingo-Pardo, G. Cortès, J. L. Taín, J. Agramunt, A. Algora, F. Ameil, Y. Ayyad, J. Benlliure, M. Bowry, F. Calviño, D. Cano-Ott, T. Davinson, I. Dillmann, A. Estrade, A. Evdokimov, T. Faestermann, F. Farinon, D. Galaviz, A. García-Ríos, H. Geissel, W. Gelletly, R. Gernhäuser, M. B. Gómez-Hornillos, C. Guerrero, M. Heil, C. Hinke, R. Knöbel, I. Kojouharov, J. Kurcewicz, N. Kurz, Y. Litvinov, L. Maier, J. Marganiec, M. Marta, T. Martínez, F. Montes, I. Mukha, D. R. Napoli, C. Nociforo, C. Paradela, S. Pietri, Zs. Podolyák, A. Prochazka, S. Rice, A. Riego, B. Rubio, H. Schaffner, C. Scheidenberger, K. Smith, E. Sokol, K. Steiger, B. Sun, M. Takechi, D. Testov, H. Weick, E. Wilson, J. S. Winfield, R. Wood, P. J. Woods, and A. Yeremin. β-decay and β-delayed neutron emission measurements at GSI-FRS beyond $N = 126$, for r-process nucleosynthesis. *Nuclear Data Sheets*, 120:81 – 83, 2014. doi: http://dx.doi.org/10.1016/j.nds.2014.07.012.

[14] K. Miernik, K. P. Rykaczewski, C. J. Gross, R. Grzywacz, M. Madurga, D. Miller, J. C. Batchelder, I. N. Borzov, N. T. Brewer, C. Jost, A. Korgul, C. Mazzocchi, A. J. Mendez, Y. Liu, S. V. Paulauskas, D. W. Stracener, J. A. Winger, M. Wolinnska-Cichocka, and E. F. Zganjar. Large β-delayed one and two neutron emission rates in the decay of ^{86}Ga. *Phys. Rev. Lett.*, 111:132502, Sep 2013. doi: 10.1103/PhysRevLett.111.132502.

[15] R. Grzywacz, K.P. Rykaczewski, C.J. Gross, M. Madurga, K. Miernik, D.T. Miller, S.V. Paulauskas, S.W. Padgett, C. Rasco, M. Wolinska-Cichocka, and Others. Hybrid-3HEN - New detector for gammas and neutrons. *Acta Physica Polonica B*, 45(2):217–222, 2014.

[16] J. Pereira, P. Hosmer, G. Lorusso, P. Santi, A. Couture, J. Daly, M. Del Santo, T. Elliot, J. Görres, C. Herlitzius, K. L. Kratz, L. O. Lamm, H. Y. Lee, F. Montes, M. Ouellette, E. Pellegrini, P. Reeder, H. Schatz, F. Schertz, L. Schnorrenberger, K. Smith, E. Stech, E. Strandberg, C. Ugalde, M. Wiescher, and A. Wöhr. The neutron long counter NERO for studies of β-delayed neutron emission in the r-process. *Nucl. Instrum. And Meth. in Phys. Res. A*, 618(1):275–283, 2010.

[17] D. Testov, D. Verney, B. Roussière, J. Bettane, F. Didierjean, K. Flanagan, S. Franchoo, F. Ibrahim, E. Kuznetsova, R. Li, B. Marsh, I. Matea, Yu. Penionzhkevich, H. Pai, V. Smirnov, E. Sokol, I. Stefan, D. Suzuki, and J. N. Wilson. The 3He long-counter TETRA at the ALTO ISOL facility. *Nucl. Instrum. And Meth. in Phys. Res. A*, 815:96 – 103, 2016. ISSN 0168-9002. doi: http://dx.doi.org/10.1016/j.nima.2015.11.150.

[18] M. B. Chadwick, M. Herman, P. Obložinský, M. E. Dunn, Y. Danon, A. C. Kahler, D. L. Smith, B. Pritychenko, G. Arbanas, R. Arcilla, R. Brewer, D. A. Brown, R. Capote, A. D. Carlson, Y. S. Cho, H. Derrien, K. Guber, G. M. Hale, S. Hoblit, S. Holloway, T. D. Johnson, T. Kawano, B. C. Kiedrowski, H. Kim, S. Kunieda, N. M. Larson, L. Leal, J. P. Lestone, R. C. Little, E. A. McCutchan, R. E. MacFarlane, M. MacInnes, C. M. Mattoon, R. D. McKnight, S. F. Mughabghab, G. P. A. Nobre, G. Palmiotti, A. Palumbo, M. T. Pigni, V. G. Pronyaev, R. O. Sayer, A. A. Sonzogni, N. C. Summers, P. Talou, I. J. Thompson, A. Trkov, R. L. Vogt, S. C. van der Marck, A. Wallner, M. C. White, D. Wiarda, and P. G. Young. ENDF/B-VII.1 Nuclear data for science and technology: Cross sections, covariances, fission product yields and decay data. *Nuclear Data Sheets*, 112(12):2887 – 2996, 2011. ISSN 0090-3752.

[19] R. Caballero-Folch, C. Domingo-Pardo, J. Agramunt, A. Algora, F. Ameil, A. Arcones, Y. Ayyad, J. Benlliure, I. N. Borzov, M. Bowry, F. Calviño, D. Cano-Ott, G. Cortés, T. Davinson, I. Dillmann, A. Estrade, A. Evdokimov, T. Faestermann, F. Farinon, D. Galaviz, A. R. García, H. Geissel, W. Gelletly, R. Gernhäuser, M. B. Gómez-Hornillos, C. Guerrero, M. Heil, C. Hinke, R. Knöbel,

I. Kojouharov, J. Kurcewicz, N. Kurz, Yu. A. Litvinov, L. Maier, J. Marganiec, T. Marketin, M. Marta, T. Martínez, G. Martínez-Pinedo, F. Montes, I. Mukha, D. R. Napoli, C. Nociforo, C. Paradela, S. Pietri, Zs. Podolyák, A. Prochazka, S. Rice, A. Riego, B. Rubio, H. Schaffner, Ch. Scheidenberger, K. Smith, E. Sokol, K. Steiger, B. Sun, J. L. Taín, M. Takechi, D. Testov, H. Weick, E. Wilson, J. S. Winfield, R. Wood, P. Woods, and A. Yeremin. First measurement of several β-delayed neutron emitting isotopes beyond $N = 126$. *Phys. Rev. Lett.*, 117:012501, Jun 2016. doi: 10.1103/PhysRevLett.117.012501.

[20] D. Testov, E. Kuznetsova, and J.N. Wilson. Response of the TETRA 4π detector to neutrons. *Journal Of Instrumentation*, 10(09):P09011, 2015.

[21] W. Królas, R. Grzywacz, K. P. Rykaczewski, J. C. Batchelder, C. R. Bingham, C. J. Gross, D. Fong, J. H. Hamilton, D. J. Hartley, J. K. Hwang, Y. Larochelle, T. A. Lewis, K. H. Maier, J. W. McConnell, A. Piechaczek, A. V. Ramayya, K. Rykaczewski, D. Shapira, M. N. Tantawy, J. A. Winger, C. H. Yu, E. F. Zganjar, A. T. Kruppa, W. Nazarewicz, and T. Vertse. First observation of the drip line nucleus ^{140}Dy: Identification of a $7\mu s$ K isomer populating the ground state band. *Phys. Rev. C*, 65:031303, 2002. doi: 10.1103/PhysRevC.65.031303.

[22] H. W. Kraner. Fast neutron damage in germanium detectors. *IEEE Transactions on Nuclear Science*, 27(1):217–234, 1980. doi: 10.1109/TNS.1980.4330831.

[23] J. Agramunt, J. L. Tain, F. Albiol, A. Algora, E. Estevez, G. Giubrone, M. D. Jordan, F. Molina, B. Rubio, and E. Valencia. A triggerless digital data acquisition system for nuclear decay experiments. *AIP Conference Proceedings*, 1541(1):165–166, 2013. doi: 10.1063/1.4810829.

[24] J. Agramunt. Briken DACQ. *3rd BRIKEN Workshop, Valencia, 22-25 July 2015*. http://indico.ific.uv.es/indico/event/briken3.

[25] Struck Innovative Systeme GmbH (www.struck.de).

[26] M. B. Gómez-Hornillos, J. Rissanen, J. L. Tain, A. Algora, K. L. Kratz, G. Lhersonneau, B. Pfeiffer, J. Agramunt, D. Cano-Ott, V. Gorlychev, R. Caballero-Folch, T. Martínez, L. Achouri, F. Calvino, G. Cortés, T. Eronen, A. García, M. Parlog, Z. Podolyak, C. Pretel, and E. Valencia. β-delayed neutron emission studies. *Hyperfine Interactions*, 223(1-3):185–194, 2014.

[27] A. Svirikhin, A Andreev, V. Dushin, M. Chelnokov, V. Chepigin, M Gupta, A. Isaev, I. Izosimov, D. Katrasev, A. Kuznetsov, O. Malyshev, A. Minkova, S. Mullins, A. Popeko, E. Sokol, and A. Yeremin. The investigation of properties of short-lived SF isotopes (Z > 100) at the focal plane of VASSILISSA separator. *EPJ Web Of Conferences*, 62:03005, 2013. doi: 10.1051/epjconf/20136203005.

[28] S. Agostinelli, J. Allison, K. Amako, J. Apostolakis, H. Araujo, P. Arce, M. Asai, D. Axen, S. Banerjee, G. Barrand, F. Behner, L. Bellagamba, J. Boudreau, L. Broglia, A. Brunengo, H. Burkhardt, S. Chauvie, J. Chuma, R. Chytracek, G. Cooperman, G. Cosmo, P. Degtyarenko, A. Dell'Acqua, G. Depaola, D. Dietrich, R. Enami, A. Feliciello, C. Ferguson, H. Fesefeldt, G. Folger, F. Foppiano, A. Forti, S. Garelli, S. Giani, R. Giannitrapani, D. Gibin, J. J. Gómez Cadenas, I. González, G. Gracia Abril, G. Greeniaus, W. Greiner, V. Grichine, A. Grossheim, S. Guatelli, P. Gumplinger, R. Hamatsu, K. Hashimoto, H. Hasui, A. Heikkinen, A. Howard, V. Ivanchenko, A. Johnson, F. W. Jones, J. Kallenbach, N. Kanaya, M. Kawabata, Y. Kawabata, M. Kawaguti, S. Kelner, P. Kent, A. Kimura, T. Kodama, R. Kokoulin, M. Kossov, H. Kurashige, E. Lamanna, T. Lampén, V. Lara, V. Lefebure, F. Lei, M. Liendl, W. Lockman, F. Longo, S. Magni, M. Maire, E. Medernach, K. Minamimoto, P. Mora de Freitas, Y. Morita, K. Murakami, M. Nagamatu, R. Nartallo, P. Nieminen, T. Nishimura, K. Ohtsubo, M. Okamura, S. O'Neale, Y. Oohata, K. Paech, J. Perl, A. Pfeiffer, M. G. Pia, F. Ranjard, A. Rybin, S. Sadilov, E. Di Salvo, G. Santin, T. Sasaki,

N. Savvas, Y. Sawada, S. Scherer, S. Sei, V. Sirotenko, D. Smith, N. Starkov, H. Stoecker, J. Sulkimo, M. Takahata, S. Tanaka, E. Tcherniaev, E. Safai Tehrani, M. Tropeano, P. Truscott, H. Uno, L. Urban, P. Urban, M. Verderi, A. Walkden, W. Wander, H. Weber, J. P. Wellisch, T. Wenaus, D. C. Williams, D. Wright, T. Yamada, H. Yoshida, and D. Zschiesche. Geant 4 – a simulation toolkit. *Nuclear Inst. And Methods in Physics Research, A*, 506(3):250–303, 2003. doi: http://dx.doi.org/10.1016/S0168-9002(03)01368-8.

[29] A. Tarifeño-Saldivia, F. Molina, J.L. Tain, D. Jordan, and L. Soto. Modelling moderated proportional neutron counters using the geant4 toolkit and the application to detection of fast neutron burst. volume PoS(XLASNPA)068, nuclear Physics, 2013.

[30] A. R. García, E. Mendoza and D. Cano-Ott. Validation of the thermal neutron physics in GEANT4. *G4 Hadronic group meeting, 17th of April 2013*.

[31] A. Tarifeño-Saldivia, C. Domingo-Pardo, J.L. Tain, A. Riego, G. Cortes-Rossel and P. Vi. Benchmark of efficiency calculations for PE moderated neutron counters. *3rd BRIKEN Workshop, Valencia, 22-25 July 2015*. http://indico.ific.uv.es/indico/event/briken3.

[32] R. Grzywacz. Beta-delayed neutrons with VANDLE: Paradise or pandemonium? *16th ASRC International Workshop "Nuclear Fission and Structure of Exotic Nuclei", Tokai, Japan, 18-20 March 2014*.

[33] M. Madurga, S. V. Paulauskas, R. Grzywacz, D. Miller, D. W. Bardayan, J. C. Batchelder, N. T. Brewer, J. A. Cizewski, A. Fijałkowska, C. J. Gross, M. E. Howard, S. V. Ilyushkin, B. Manning, M. Matŏs, A. J. Mendez, K. Miernik, S. W. Padgett, W. A. Peters, B. C. Rasco, A. Ratkiewicz, K. P. Rykaczewski, D. W. Stracener, E. H. Wang, M. Wolinska-Cichocka, and E. F. Zganjar. Evidence for Gamow-Teller decay of ^{78}Ni core from beta-delayed neutron emission studies. *Phys. Rev. Lett.*, 117: 092502, Aug 2016. doi: 10.1103/PhysRevLett.117.092502.

[34] Froehner, F.H. Watt spectrum fit to 252Cf prompt fission neutron data. In *IAEA-TECDOC–483, 160-164*, 1988.

[35] L. Mathieu, O. Serot, T. Materna, A. Bail, U. Köster, H. Faust, O. Litaize, E. Dupont, C. Jouanne, A. Letourneau, and S. Panebianco. New neutron long-counter for delayed neutron investigations with the LOHENGRIN fission fragment separator. *Journal Of Instrumentation*, 7(08):P08029, 2012.